Journal of Environment and Earth Science
ISSN 2224-3216 (Paper) ISSN 2225-0948 (Online)
Vol.5, No.22, 2015
www.iiste.org

Mineralogy and Fluid Inclusions of the Kettara Massive Sulphide Deposit (Jebilet Massif, Variscan Belt, Morocco)

Ismaïla N'Diaye[1], Abderrahim Essaifi[1], Michel Dubois[2], Brice Lacroix[3]

1. DLGR, Geology Department, Cadi Ayyad University, B.P. 2390, Marrakech 40000, Morocco
2. LGCgE, Bâtiment SN5, Université Lille 1, 59655 Villeneuve d'Ascq, France,
3. Institut des Sciences de la Terre, Université de Lausanne, 1015 Lausanne, Switzerland

Abstract

The Kettara copper deposit is located in the centre of the Jebilet massif, north of Marrakech, and consists of an elongated sub-vertical pyrrhotite-rich massive sulphide lens. The host rocks consist of thin-bedded Visean pelites with sandstones, calcareous beds and doleritic dykes. The host rocks have been folded, foliated, and metamorphosed to low greenschist facies conditions during the Variscan orogeny.

The sulphide mineralization comprises a main lens composed of massive to semi-massive pyrrhotite accompanied by chalcopyrite, magnetite, sphalerite, arsenopyrite, galena and a quartz-chlorite gangue, centimetre-scale mineralized syntectonic replacement veins in the wall rocks with the same mineralogy as the main lens, and a later pyrite-carbonate veins that cut across pyrrhotite mineralization. Microthermometry and Raman analysis indicate that the mineralizing fluids associated with pyrrhotite formation were H_2O, N_2, CH_4 and CO_2-bearing, with low salinities (7.5 wt.%NaCl), typical for low-grade metamorphism. *P-T* conditions from fluid inclusion studies and chlorite geothermometry indicate that pyrrhotite formation occurred at c. 200-400°C and c. 2 kbar. These characteristics indicate that the genesis of the main mineralization in the Kettara massive sulphide deposit might have taken place in the transition between diagenetic and metamorphic environments or in metamorphic environment under reducing condition.

Keywords: massive sulphide, pyrrhotite, fluid inclusions, deformations.

1. Introduction

The Kettara deposit is a sedimentary-hosted massive sulphide deposit, located in the Central Jebilet massif (north of Marrakesh), which comprises a Carboniferous sedimentary sequence that was weakly metamorphosed, deformed and intruded by a range of magmatic rocks during the Variscan orogeny (Figure 1). The deposit consists of an elongated lens, about 1.5 km long, 500 deep with an average thickness of 11 m, but can locally reach 70 m (Fournier *et al.* 1987; Bernard *et al.* 1988). The mineralogy is dominated by fine-grained pyrrhotite, together with magnetite, pyrite, chalcopyrite, sphalerite and accessory galena and arsenopyrite (Huvelin 1970; Bernard *et al.* 1988; Essaifi & Hibti 2008). The gangue minerals are essentially quartz, chlorite, siderose and micas (Huvelin 1970). At the surface, weathering of sulphides has generated a well-developed gossan that can be traced to a depth of 50 m and was exploited for limonite and ochre from 1938 to 1963. The extracted quantities are respectively 150 000 t grading 45-52% Fe and 50 000 t grading 50-58 % Fe (Essaifi 2011 and references therein). A cementation zone with mineralization composed of native copper, pyrite, chalcocite (Cu_2S), covellite (CuS) and traces of gold and silver occurs below the gossan (Souaré 1988). Pyrite was extracted from this zone between 1955 and 1966, and used in the manufacture of sulphuric acid with recuperation of Cu contained in chalcocite and covellite. Its total reserves have been estimated to 180 000 t grading 38% S. Below the cementation zone, the primary mineralization is pyrrhotite-rich (up to 95%) and extends to 500 m deep (Huvelin 1970). The ore reserves are estimated to 30 Mt of pyrrhotite grading 0.7% Cu; 8 Mt were extracted from 1964 to 1982 and used in the manufacture of sulphuric acid. Difficulties related to pyrrhotite storage (fast oxidation), poor sulphur content (25%), and to the volume of mine wastes resulted in the closure of the mine in 1982.

The Kettara deposit was the first massive sulphide deposit that has been discovered in the Jebilet massif in the 1930s. Since then, numerous other massive sulphide deposits have been discovered in the region, including Draa Sfar, Koudiat Aïcha, and also the Hajjar deposit at the southern prolongation of Jebilet massif. The Kettara massive sulphide deposit has been interpreted as a mineralized dyke filling a subvertical fracture (Agard *et al.* 1952) or as a pre-tectonic deposit probably emplaced contemporaneously with deposition of sediments (Huvelin 1970). Since then, different studies have been carried out on different massive sulphide deposits of the area, but their genesis still remains a subject of discussion. They are considered as syngenetic exhalative (Bernard *et al.*

1988), either VMS (Marcoux *et al.* 2008; Belkabir *et al.* 2008) or SEDEX deposits (Moreno *et al.* 2008, Lotfi *et al.* 2008) or transitional between VMS and SEDEX deposits (Hibti & Marignac 2001). Essaifi *et al.* (1995) and Essaifi & Hibti (2008) evoke an epigenetic genesis of the massive sulphide deposits of the Jebilet massif by fluid migration through shear zones and a possible genetic relationship between the massive sulphide deposits and a Variscan bimodal plutonism present in the area.

This contribution presents a new investigation of the abandoned Kettara mine including new geological, mineralogical and fluid inclusions data in order to constrain the genesis of the Kettara massive sulphide deposit.

2. Geological setting

The Kettara deposit is located 35 km NW of Marrakech, in the central unit of the Jebilet massif, in the western Moroccan Meseta (Figure 1a). The Jebilet massif is oriented E-W, and is subdivided into three structural units separated by major shear zones (Huvelin 1977; Lagarde & Choukroune 1982; Le Corre & Bouloton 1987; Essaifi *et al.* 2001) : (i) the western unit is formed by unmetamorphosed Cambro-Ordovician limestones, shales and sandstones; (ii) the eastern unit is composed of unmetamorphosed to weakly metamorphosed upper Visean sediments (Kharrouba Flysch); (iii) the central unit, where the Kettara deposit is located, is formed by upper Visean-Namurian detrital sediments (Sarhlef schists), deformed and metamorphosed under low greenschist facies conditions (Figure 1b). The original sediments of central Jebilet were deposited in an anoxic platform (Beauchamp 1984) in a Devonian to early-Carboniferous foreland basin of age (Bouabdelli & Piqué1996). Basin closure occurred during a post-Visean crustal shortening, leading to deformation and metamorphism (Piqué & Michard 1989; Hoepffner *et al.* 2006). The central unit of Jebilet is also characterized by important syntectonic magmatism comprising an ultramafic to granitoid bimodal association (>65% mafic−ultramafic, the remainder is felsic), associated with peraluminous granodiorites emplaced at c. 330 Ma, intruded by younger (300 Ma) leucogranites (Mrini *et al*. 1992; Essaifi *et al.* 2014). Microdioritic dykes post-date the major Variscan folds (Huvelin 1977).

Metamorphism in central Jebilet is epizonal. It is characterized by the development of sericite, chlorite, quartz, epidote, and sporadically biotite, corresponding to greenschist facies conditions (Huvelin 1977; Bordonaro 1983). This metamorphism was contemporaneous with the Variscan ductile deformation, developed during the post-Visean crustal shortening, which is the major tectonic event in the Moroccan Meseta (Hoepffner *et al.* 2006). The regional ductile deformation is characterized by a NE-SW S_1 cleavage, which is axial planar to large subhorizontal folds, and the development of anastomosing shear zones (Essaifi *et al.* 2001) (Figure 1c). The major Variscan deformation was followed by a late folding phase accompanied by kink bands and a crenulation cleavage (Huvelin 1977). A brittle deformation marked by E-W faults is superimposed on the ductile deformation.

3. Methods and analytical procedures

The collected data and description of structures, textures and mineralogy of the ore body is based on detailed field descriptions of the Kettara deposit and its country rocks, borehole observations and on samples collected from natural exposures and the ore stockpile present on the mine site. The minerals were analyzed by FEI Quanta200-scanning electronic microprobe (SEM) with Bruker diode EDX, Xflash 3001 at the University of Lille 1. The chemical compositions of sulphide minerals were taken from Souaré (1988) unpublished thesis, while chlorite associated with sulphides has been analyzed at the University of Lausanne using a JEOL 8200 superprobe electron microprobe equipped with five X-ray spectrometers on coated thin sections. The microprobe operated at 15 kV with a current of 10 nA and a beam diameter of 3 µm. The standards used were Wollastonite (Si, Ca), Andalusite (Al), haematite (Fe), Forsterite (Mg), Albite (Na), Orthose (K) and MnTi (Mn, Ti).

Fluid inclusions were studied from two samples including a quartz mineralized vein crosscut by carbonates ($V_{m\text{-}qc}$) and a quartz-chlorite mineralized vein ($V_{m\text{-}qcl}$); both are parts of the main mineralization of the Kettara deposit. In order to characterize fluid compositions, microthermometry and Raman microspectrometry on fluid inclusions have been used. Microthermometry was performed at Cadi Ayyad University using a Chaix meca microthermometry apparatus (Poty *et al.* 1976), calibrated using standard synthetic fluid inclusions: i/ H_2O-CO_2 inclusions with the melting of solid CO_2 at -56.6°C, ii/ pure H_2O inclusions (ice melting at 0.0°C, and critical homogenization temperature at 374.1 °C), and iii/ H_2O-NaCl inclusions with eutectic at -21.2 °C. These data were completed at the University of Lille 1 by additional microthermometric measurements obtained using a FLUID INC (USGS-type) heating and freezing stage, calibrated using the same standards. The precision of

measurement is ±0.1 and ±0.5 at low- and high-temperature respectively. Salinities were calculated from $T_{m(ice)}$ using the empirical equation of Bodnar (1993) and Bodnar & Vityk (1994). Semi-quantitative compositional data of inclusion vapor bubbles were determined from Laser Raman spectra obtained at the University of Lille 1, by using the method summarized in Frezzotti *et al.* (2012). The Raman spectra were recorded with a LabRam HR800 Jobin-Yvon microspectrometer equipped with 1800 g/mm gratings and using 532.28 nm (green) laser excitation. Acquisition time span varied from 20 to 60 s during three accumulating cycles. The spectra regions scanned were in the range of 1000-1500 cm^{-1} for CO_2, 2250-2750 cm^{-1} for N_2 and H_2S and 2750-2950 cm^{-1} for CH_4.

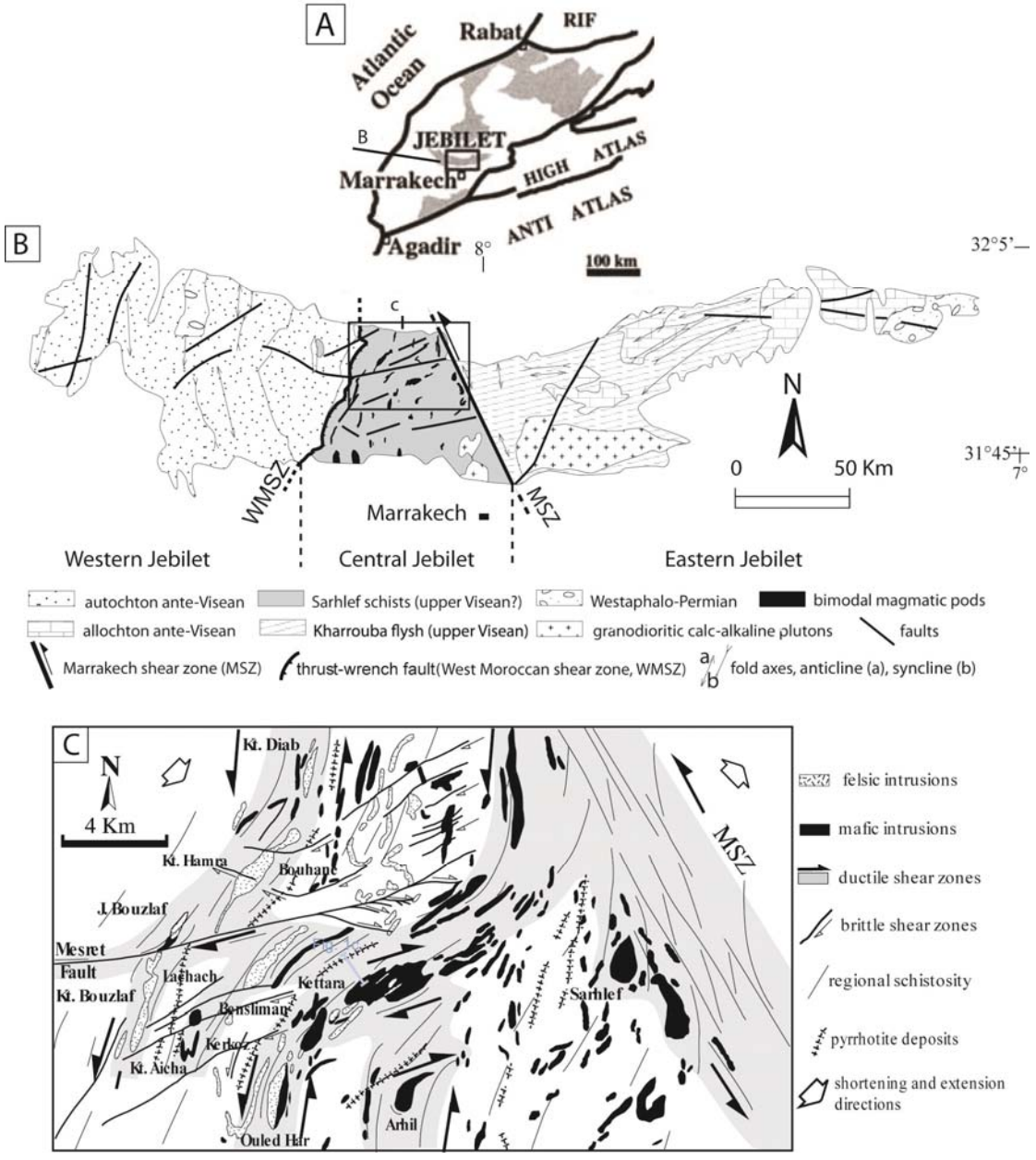

Figure 1. General location of the studied area. (A) Location of the Jebilet massif in the Moroccan structural domains. (B) Simplified geological map of Jebilet massif (modified after Huvelin (1977)). (C) Location of the Kettara intrusion and the Kettara massive sulphide deposit. Note that both the deposit and the intrusion are located in a shear zone interconnected with regional anastomosed shear zones (after Essaifi and Hibti 2008)

4. Geology of the Kettara massive sulphide deposit

The Kettara deposit forms a sub-vertical pyrrhotite-dominated massive sulphide lens elongated concurrently to the NE-SW regional structural trend (Essaifi and Hibti 2008), and represented at the surface by a well-developed gossan that extends to depths of c. 50 m. It is hosted within the Sarhlef schists of the central Jebilet block, and crops out approximately one km NW of the mafic-ultramafic Kettara intrusion, part of the central Jebilet bimodal magmatic association (Figure 2).

4.1. Host rocks

The central Jebilet terrane (Sarhlef schists) are weakly metamorphosed pelites with thin-bedded sandstone and locally sandstone and limestone layers (± 10 m in thickness). In the Kettara area, these schists which are devoid of any volcanic units, dip steeply (70-80°) north-west, and are right-way-up. The Kettara deposit also dips steeply to the NW, allowing us to describe the host schists to the south of the gossan as the footwall and those to the north of the gossan as the hanging wall of the deposit.

- The host rocks located on the southern side of the deposit, i.e. between the Kettara intrusion and the massive sulphide deposit (~1000m of footwall lithofacies), are dominantly composed of black pelites and subvertical intercalated thin beds of fine-grained sandstone. They are cross-cut by doleritic dykes and affected by a well-developed schistose fabric (Figure 2). Approaching the deposit the pelites become light grey then green and the sandstone beds become progressively thinner while the bedding planes (S_0) are totally transposed into the schistose fabric (S_1). The pelites are dominated by a muscovite-quartz-chlorite-albite mineral assemblage, with muscovite being the most abundant mineral. At the margin of the deposit muscovite (sericite) is aligned along the schistosity plane (S_1) while far from the deposit some muscovite grains are oblique to S_1 and show pressure shadows. Fe-rich chlorite appears at a distance of 10 m from the deposit and its abundance increases towards the deposit. In the sandstone layers, mineralogy is dominated by quartz and feldspar. In the sandstones quartz has an average grain size of 50 µm and forms up to 95 vol. % of the rock. Strain intensity increases towards the deposit where original stratification is obliterated by schistosity accompanied by the development of kink band structures.

- The host rocks located on the northern side of the deposit, i.e. the hanging wall lithofacies, are composed of fine-grained pelites enclosing calcareous and siltstone intercalations, and crosscut by doleritic dykes (Figure 2). They consist of dark grey pelites that become light grey near the deposit with a mineralogy dominated by a quartz-chlorite-muscovite-albite assemblage. Sericite and chlorite abundance increase towards the contact with the deposit. The calcareous intercalations evolve progressively from centimetre- to metre-scale S-shaped lenses of fine-grained bioclastic limestone and calcareous sandstone close to the deposit to a coarse-grained layered calcareous sandstone bed located 1.5 km from the deposit. This calcareous bed is a 10 metre-thick stratigraphic marker in the area; it strikes parallel to a metre-scale dyke of microgabbro located c. 1000m to the south. The calcareous lenses are composed of calcite, bioclast fragments (ooliths) and xenomorphic or recrystallized quartz grains. The average grain size of quartz in the sandstone beds is 25 µm, in contrast with the more coarse-grained sandstones in the footwall. As in the footwall, strain intensity increases towards the deposit where the calcareous intercalations are boudinaged and transposed into the schistosity plane. The lithofacies of the hanging wall are generally affected by post-schistosity fractures filled with calcite and ferrous oxides.

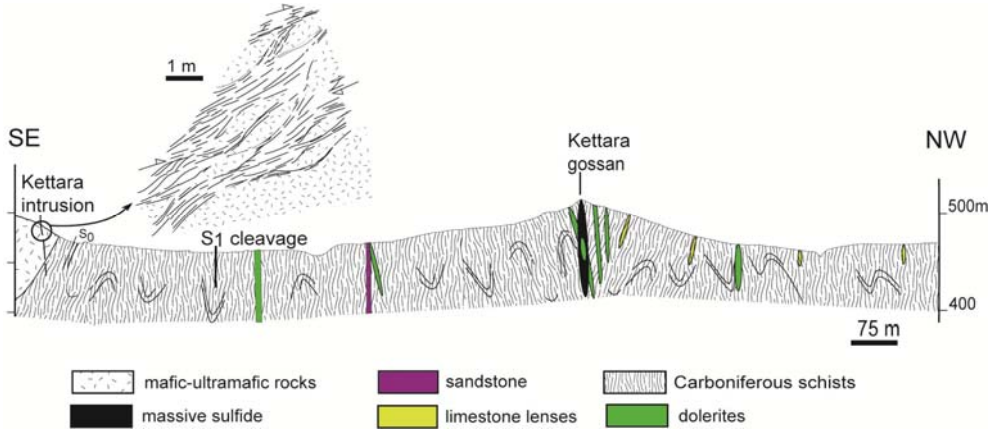

Figure 2. Vertical cross-section through the Kettara deposit. See location in Figure 1c. The diagrammatic section illustrates metre-scale shear zones in the Kettara mafic-ultramafic intrusion

4.2. Massive sulphide mineralization

The Kettara massive sulphide deposit is composed of several ore types differently named in previous studies (Huvelin 1970; Bernard *et al.* 1988; Hibti *et al.* 1999; Essaifi & Hibti 2008). The structures, textures and mineralogy analysis of the ores allowed us to distinguish three main types (Figure 3).

- *Massive to semi-massive pyrrhotite ore* is the most abundant type and is found at depths below 50m (Figure 3a). It is composed of massive pyrrhotite (70-90%), chalcopyrite (5-25%), magnetite (3-5%), sphalerite (2%), arsenopyrite (<1%) and traces of galena and native bismuth. The gangue minerals are quartz and chlorite, sometimes accompanied by talc and mica, or encloses phosphate minerals and Ti-oxides. The semi-massive ore is characterized by a chlorite-rich gangue and a mylonitic fabric formed during the regional deformation in the Jebilet massif. Pyrrhotite forms lenses concordant with the host chlorite-schists and show often a kink band structures. It also includes interstratified fragments of schists and millimetre-scale beds of recrystallized quartz. These structures have been interpreted as due to the replacement of the host schists by the mineralizing fluid (Moreno *et al.* 2008). On the surface the gossan cuts across a doleritic dyke and meter-scale lenses of dolerite are enclosed by massive pyrrhotite (Huvelin 1970; Fournier *et al.* 1987). The pyrrhotite ore is cross-cut by carbonate-filled ‘‘en echelon’’ veins and fractures.

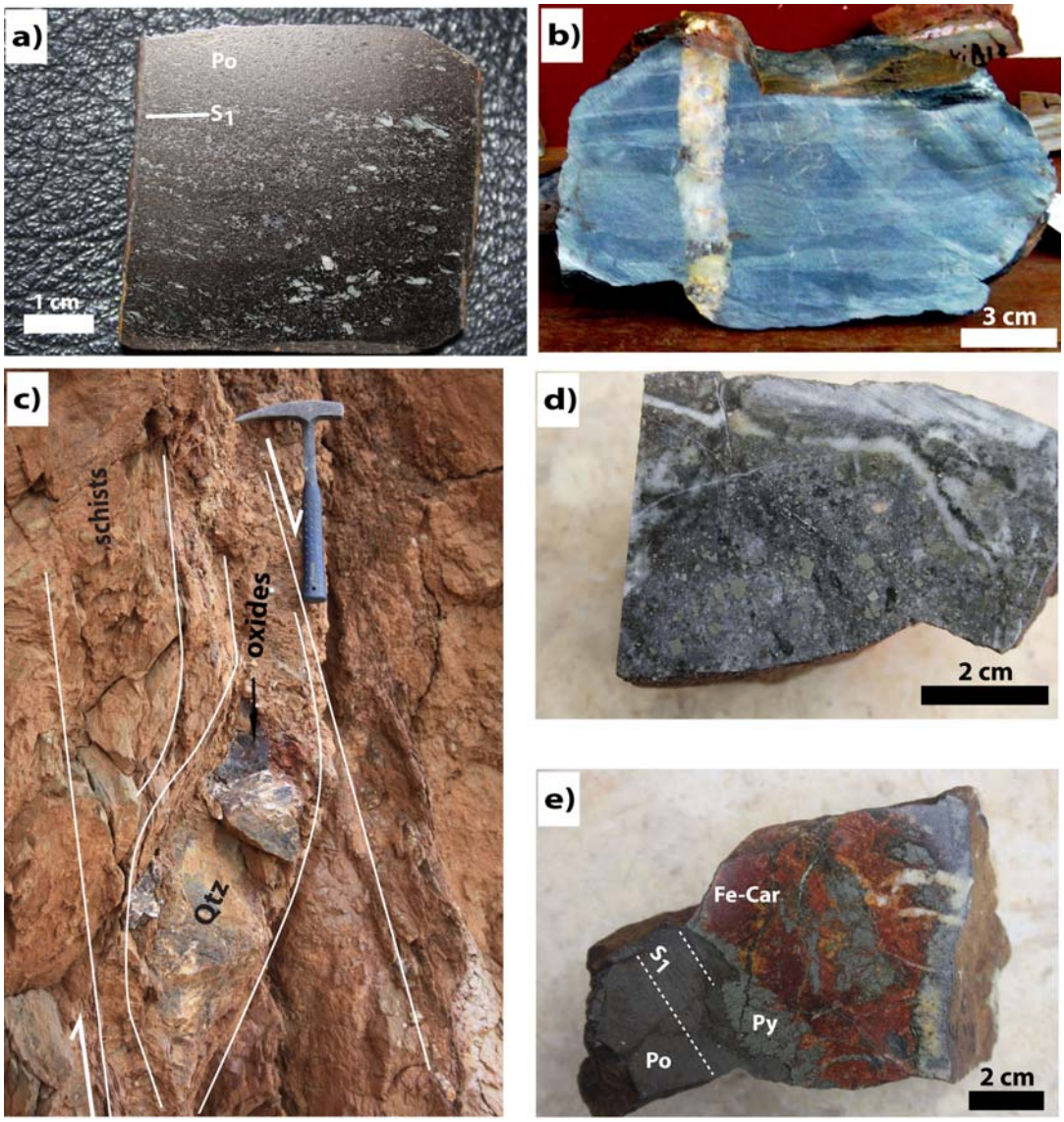

Figure 3. Photographs of polished ore samples of the Kettara massive sulphide deposit. a) Massive pyrrhotite (Po) enclosing chlorite and white mica (white) elongated along the S_1 cleavage. b) Quartz (white) mineralized vein crosscutting wall rocks composed of alternating pelites (black) and sandstone (grey) layers. Note that

mineralization within the vein lie in continuity with the pelite layers. c) Vertical sigmoidal quartz-vein with mineralization oxidized, in the footwall. d) Pyritic ore showing euhedral pyrite weakly fractured to angular grains. e) Replacement of pyrrhotite (Po) by pyrite (Py) and carbonates (Car). Note that pyrite is discordant on the S_1 cleavage that affects the pyrrhotite-rich zone

- *Mineralized veins* are mainly pyrrhotite-rich quartz-chlorite mineralized veins, and are developed in the wall rocks principally in the footwall. They are centimetre-scale massive veins with gradational to sharp boundaries (Figure 3b, c). The veins have a mineralogy similar to that of the massive pyrrhotite ore, being composed of a quartz-chlorite gangue enclosing pyrrhotite, chalcopyrite, sphalerite, arsenopyrite, galena, and native bismuth. Phosphate minerals and zircon are also found in the pyrrhotite mineralized veins. Despite weathering at the surface, oxidized chalcopyrite is observed in sigmoidal quartz veins in the footwall (Figure 3c). The veins cross-cut the layering in the host schists, which is composed of millimetre-scale pelite and sandstone layers transposed in the foliation plane. The veins do not entirely postdate the foliation; they show a ductile deformation marked by grain boundary sliding in quartz grains and orientation of sulphide minerals along the foliation plane. The sulphide minerals develop in layers that are in continuity with the pelite layers of the host schists. They occur between the quartz grains or in association with chlorite in the vein margins. The sulphide minerals, especially pyrrhotite, are also present in the host schists around the veins where they are localised along the foliation plane in the pelites. Thus the pelite banding persists through the veins by alternation of sandstone layers composed of fine-grained quartz (0.1 mm) and layers composed of coarse-grained quartz associated with chlorite and sulphides which have replaced former pelite layers. We interpret these veins as replacement veins formed by local alteration of wall rock along fractures during the end of the ductile deformation phase. Bernard *et al*. (1988) described quartz-calcite veins associated with metasomatic chloritites in the wall rocks of the Kettara deposit.

- *Pyritic ore* consists of a pyrite-rich mineralization that occurs generally as cm-scale veins or pods crosscutting the massive to semi-massive pyrrhotite. It is composed of centimetre-scale brecciated pyrite together with rare marcasite and chalcopyrite associated with a gangue of carbonates (Figure 3d). The carbonates and associated sulphides form ribbons and fracture-fills replacing the massive to semi-massive pyrrhotite (Figure 3e), the pyrrhotite mineralized veins and the host schists. So the pyritic ore encloses pockets of quartz-chlorite and relicts of pyrrhotite. Pyrrhotite is also disaggregated by carbonates associated with sub-euhedral pyrite. The pyritic ore has been affected by brittle deformation but is unaffected by ductile deformation. Pyrite crystals are locally fractured and brecciated, but lack features associated with ductile deformation such as pressure shadows. Undeformed euhedral crystals of pyrite are also disseminated in the hanging wall or form thin bed layers interstratified in the host rocks

4.3. Ore microscopy and mineral chemistry

Pyrrhotite in the massive to semi-massive ore forms elongated grains up to one millimetre in size enclosing chlorite fragments oriented along the schistosity plane (Figure 4a). Equigranular grains of pyrrhotite, c. 0.01mm in size, presenting 120° triple junctions, are also observed (Figure 4b). Pyrrhotite associated with chalcopyrite often fill fractures in magnetite (Figure 4c), or are localized along C/S planes in the mylonitic semi-massive ore. Pyrrhotite associated with chalcopyrite and/or magnetite are sometimes kinked in the massive to semi-massive ore. In the pyrrhotite mineralized veins, pyrrhotite grains, 1-3 mm in size, crystallize in association with Fe-rich chlorite along the vein margins and between quartz grains in the centre of the veins. In the pyritic ore, pyrrhotite is present as relicts inside the Fe-rich carbonate-pyrite association (Figure 4d). Scanning electronic microscopy allowed identification of 3 to 10 µm-long inclusions of *native bismuth* disseminated within pyrrhotite in both the massive ore and the mineralized veins. The composition of pyrrhotite is relatively constant (Table 1), with a stochiometric formula close to Fe_7S_8 and atomic Fe contents (≈ 46.31 ± *0.22* %) similar to those of monoclinic pyrrhotite (Arnold 1966). Pyrrhotite in the Kettara deposit is Ni- and Co-free but contains up to 4000 ppm Pb and 300 ppm Se while the contents of these elements in pyrrhotite generally do not exceed 28 and 100 ppm respectively (Vaughan and Craig 1978).

Chalcopyrite represents 5 to 25 vol. % of the semi-massive to massive ore where it forms isolated crystals or grains associated with pyrrhotite, and/or sphalerite and magnetite. It is generally oriented, together with pyrrhotite and sphalerite, along the schistosity (S_1) and shearing planes. Chalcopyrite is sporadically present as recrystallized hexagonal grains (0.02 mm in size). Chalcopyrite blebs (chalcopyrite disease; Barton 1978) are present within sphalerite in massive to semi-massive ore and pyrrhotite mineralized veins (Figure 4e).

Chalcopyrite also shows textures of replacement by the carbonate-pyrite association (Figure 4d, f - Figure 5a). Remobilized chalcopyrite fills fractures cross-cutting pyrite in the pyritic ore (Figure 5b-c). The average contents of Cu, Fe and S in chalcopyrite are respectively 25.05 atom.% 25.24 atom.% and 49.56 atom.% (Table 1). The detected trace elements are Co, Ni, As, Ag, Pb and Zn. Like in pyrrhotite, the average concentration of Pb in chalcopyrite (1695 ppm) exceeds the values normally expected in chalcopyrite (62 ppm, Vaughan & Craig 1978). Such high Pb contents are recorded in the other sulphide minerals of the Kettara deposit (see below), and could result from the presence of very fine inclusions of galena within these minerals and/or a surface contamination of the samples.

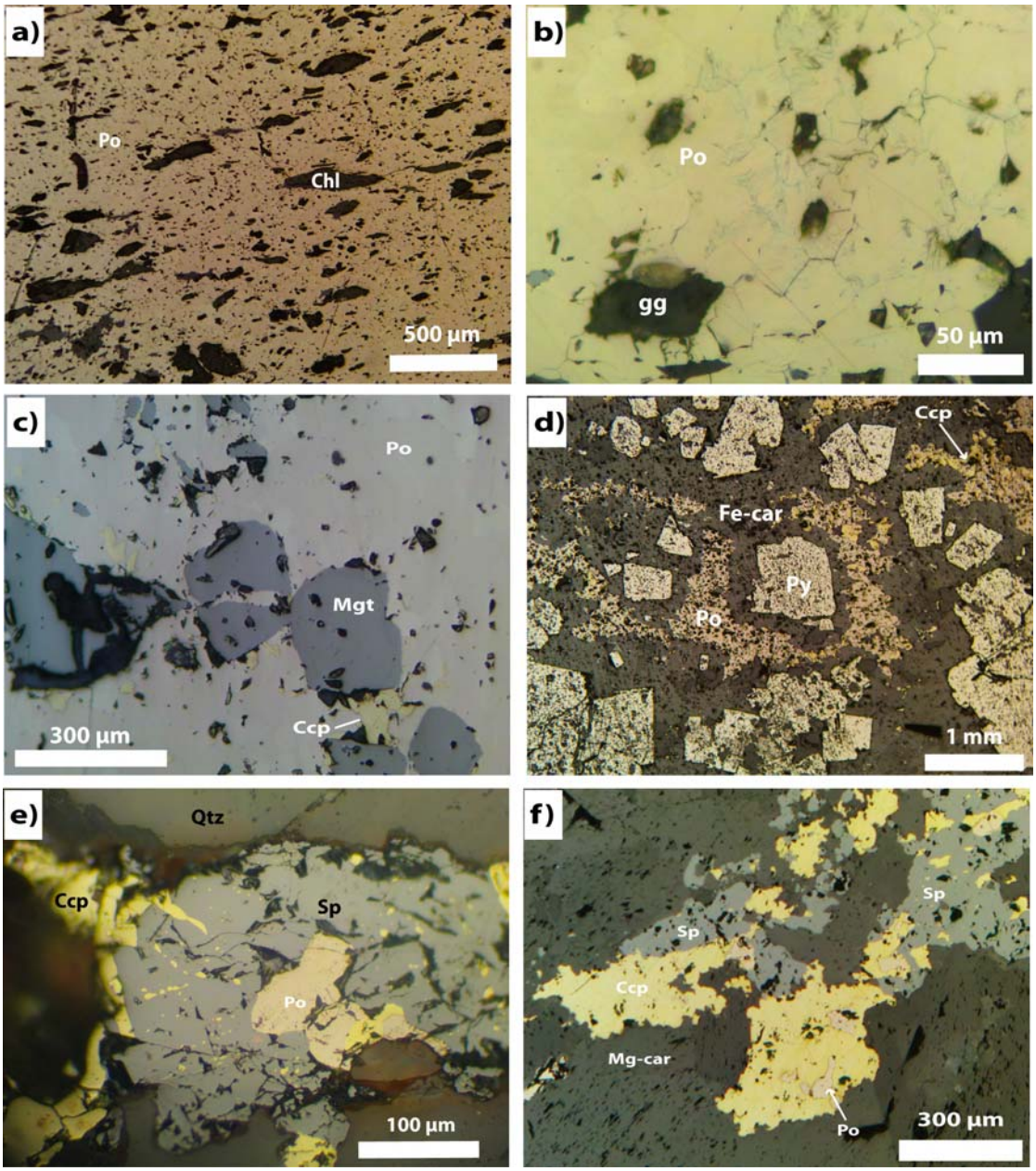

Figure 4. Reflected, plane-polarized light photomicrographs of the Kettara pyrrhotite-rich ore. a) massive pyrrhotite (Po) ore with chlorite (Chl) elongated along schistosity (S_1) planes, b) massive pyrrhotite showing annealing texture with 120° triple junctions. Note that boundaries of pyrrhotite grains are altered to oxides (white grey), gg: gangue, c) euhedral magnetite (Mgt) with fracture filled by pyrrhotite, d) replacement of a pyrrhotite-chalcopyrite (Ccp) assemblage by Fe-rich carbonates (Fe-Car) and euhedral pyrite (Py), e) chalcopyrite disease within fractured sphalerite (Sp), f) polymetallic assemblage of chalcopyrite, sphalerite, pyrrhotite in massive ore replaced by Mg-rich carbonates (Mg-Car)

Pyrite is the principal sulphide of the pyritic ore where it is present as cataclastically deformed grains (≤5 mm in size) (Figure 5b-c). Such a texture characterizes comminution breccias in brittle to semi-brittle shear zones (Brown & McClay 1993). These cataclastically deformed pyrite zones are sealed by carbonates. Pyrite can be associated with marcasite along fractures where they replace quartz-pyrrhotite association in mineralized veins (Figure 5d). In zones preserved from deformation, pyrite that replaces pyrrhotite can be limpid, sub-euhedral, undeformed and fracture-free. Euhedral pyrite has locally crystallized along margins of fractures sealed by carbonates in pyrrhotite mineralized veins (Figure. 5e). Pyrite also crystallizes along cleavage planes of ankerite and forms alternating lamellae with carbonates in pyrrhotite mineralized veins (Figure 5f). Fe contents in pyrite vary from 32.53 to 36.84 atom.% while S varies from 63.16 to 67.43 atom.%. Among the detected trace elements in pyrite (Pb, Ni, As, Ag and occasionally Cu, Zn and Se), Pb has the highest concentration with contents varying from 630 to 4900 ppm while Ni contents vary from 40 to 1390 ppm. Pyrite in Kettara is Co-free.

Sphalerite occurs in the massive to semi-massive pyrrhotite ore where it forms a polymetallic association with pyrrhotite, chalcopyrite and/or magnetite, and fills veins inside pyrrhotite. The polymetallic association is replaced by Mg-rich carbonates invading the massive ore (Figure 4f). In the pyrrhotite mineralized veins, sphalerite associated with pyrrhotite and chalcopyrite is present as fractured grains (0.15 mm in size) (Figure 4e). Sphalerite composition is relatively constant with 45.35 ± 0.20 atom.% Zn, 48.85 ± 0.32 atom.% S and 5.75 ± 0.29 atom.% Fe (Table 1). The detected trace elements are Ni, As, Sb, Cu and Pb. Lead content varies between 400 and 1610 ppm.

Arsenopyrite is present in the massive ore as sub-euhedral to euhedral microcrystals (0.05 mm in size) associated with pyrrhotite and/or chalcopyrite. Sub-euhedral arsenopyrite within massive pyrrhotite is locally enveloped by chalcopyrite. Acicular arsenopyrite is scarce; it can be associated with chalcopyrite and/or sphalerite. 0.14 mm-long micro-crystals of arsenopyrite disseminated within pyrrhotite are locally observed, and they are crosscut by fractures filled with carbonates.

Galena and Marcasite are encountered sporadically. Galena (<1 vol. %) occurs as fine grains (≈ 0.05 mm in size) disseminated within pyrrhotite in the massive ore while marcasite (<1 vol. %) is present as fractured crystals (≈ 0.1 mm in size) associated with pyrite along fractures cross-cutting pyrrhotite. The average contents of Pb and S in galena are 49.75 and 49.64 atom.% respectively. The detected trace elements are principally Fe, Co, Ag, Sb and Se, and less frequently Zn and As. Fe content in galena is high (0.11-0.34%) and exceeds the maximum value recorded in galena (0.10%, Vaughan & Craig 1978).

Oxides, principally magnetite and haematite, are associated with the sulphide minerals in the Kettara deposit. Magnetite is present in the massive pyrrhotite ore where it occurs as euhedral (0.001-2 mm), often fractured crystals (Figure 4c). Pyrrhotite and chalcopyrite fill these fractures indicating a primary origin of magnetite. Its presence indicates that the mineralizing fluid is Fe-rich. Haematite develops along mineral boundaries as an alteration mineral. In the wall rocks, Ti-oxides (anatase, rutile) and haematite occur as pre-tectonic disseminated minerals in the host schists. Ti-oxides are also found as relicts in chlorites associated with the massive to semi-massive pyrrhotite.

Gangue minerals associated with the massive sulphides are principally chlorite, quartz and carbonates and sometimes talc and mica. Quartz and chlorite are associated with pyrrhotite whereas carbonates are associated with pyrite. The chlorite has been analyzed in two samples, a semi-massive sulphide ore where chlorite is the dominant gangue mineral and a quartz-chlorite mineralized vein where chlorite is located at the vein margins. The chlorites associated with these sulphides consist of iron-rich chlorites with X_{Fe} values (X_{Fe}=Fe/(Fe+Mg)) between 0.63 and 0.74 (Table 2). Using Kranidiotis & Mac Lean (1987) geothermometer, these chlorites show a temperature of formation ranging from 347 to 370 °C for massive to semi-massive ore and from 325 to 342 °C for mineralized veins, with mean values of 360 and 330 °C, respectively.

Fe- and Mg-rich carbonates develop at the expense of pyrrhotite while Ca-rich carbonates are scarce. The Fe-rich carbonates are accompanied by pyrite while the interface between Mg-rich carbonate and pyrrhotite is pyrite-free (Figure 4d, f - Figure 5a).

Scanning electronic microscopy (SEM) allowed identification of phosphate minerals with trace elements (Ce, La, Ca) in both the massive to semi-massive ore and the pyrrhotite mineralized veins. Zircon has also been detected in the mineralized veins while talc was detected in the pyrrhotite of massive ore.

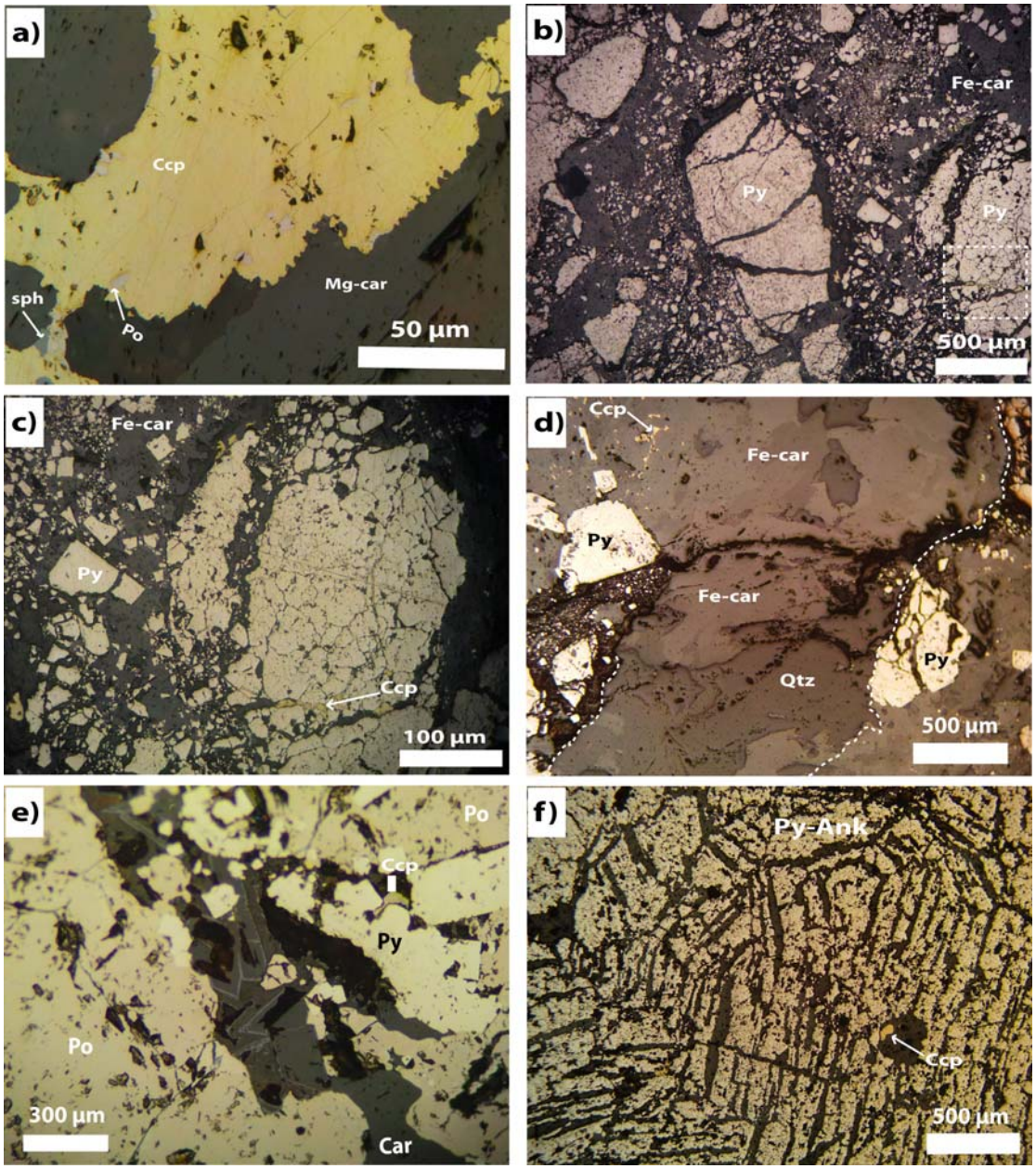

Figure 5. Reflected, plane-polarized light photomicrographs of the Kettara pyrite-rich ore. a) Mg-rich carbonates (Mg-car) replacing chalcopyrite in massive ore, b) Cataclastic deformation of pyrite resulting in comminution breccias sealed by Fe-rich carbonates (Fe-car) (see picture c for details in dashed frame), c) Cataclastic deformation of pyrite showing remobilized chalcopyrite sealing fractures (dashed frame in picture b), d) previous quartz vein (dashed lines) cross-cut by a fracture filled by pyrite and Fe-rich carbonates (Fe-car). The quartz which is normally associated to pyrrhotite is quasi-totally replaced by carbonates at the top of the picture, e) Carbonate-pyrite veinlet cutting across massive pyrrhotite in quartz mineralized vein. Pyrite develops in the margins of the vein by replacement of pyrrhotite and haematite lamellae develop along cleavage planes of carbonates, f) guided replacement of pyrite by cleavage planes of ankerite (Ank)

Table 1. Electron microprobe analyses of sulphide minerals from the Kettara deposit (from Souaré 1988).

(A) Pyrrhotite

Samples	1	2	3
Fe wt.%	58.92	58.77	58.94
S	39.38	39.15	38.82
Co (ppm)	0	0	0
Ni	0	0	0
As	0	0	80
Ag	0	0	150
Sb	0	210	0
Cu	0	210	100
Pb	4000	1040	2440
Zn	0	960	120
Se	190	300	40
Total wt.%	98.71	98.19	98.05
Fe %at	46.16	46.23	46.53
S %at	53.75	53.65	53.39
Pb %at	0.08	0.02	0.05
Structural formulae			
Fe	0.92	0.92	0.93
S	1.07	1.07	1.07
Fe/S	0.86	0.86	0.87

(B) Sphalerite

Sample	1	2	3
Zn wt.%	61.49	60.96	61.18
Fe	7	6.51	6.39
S	32.25	32.57	32.17
Co (ppm)	90	0	0
Ni	0	70	170
As	150	120	0
Ag	0	0	0
Sb	170	40	40
Cu	0	160	150
Pb	1610	1020	400
Se	90	0	0
Total wt.%	101.5	100.8	100.4
Zn %at	45.37	45.13	45.55
Fe %at	6.05	5.64	5.57
S % at	48.52	49.17	48.84
Pb %at	0.04	0.02	0.01
Structural formulae			
Zn	0.91	0.9	0.91
Fe	0.12	0.11	0.11
S	0.97	0.98	0.98
mole%FeS	12.28	11.47	11.77

(C) Chalcopyrite

Sample	1	2
Cu Wt.%	34.26	33.93
Fe	30.14	30.24
S	33.96	34.1
Co (ppm)	10	870
Ni	120	390
As	200	30
Ag	770	790
Sb	0	0
Pb	1560	1830
Zn	80	70
Mn	150	0
Se	0	0
Total wt.%	98.64	98.58
Cu %at	25.19	24.92
Fe %at	25.21	25.27
S %at	49.49	49.64
Structural formulae		
Cu	1.01	1.00
Fe	1.01	1.01
S	1.98	1.99

(D) Pyrite

Sample	1	2	3	4	5	6	7	8	9	10	11	12	13
Fe Wt.%	46.46	45.71	46.97	45.98	46.38	46.69	46.76	45.85	46.71	46.28	46.69	50.44	46.2
S	53.69	54.15	53.47	53.78	53.54	52.73	52.43	53.19	52.45	52.47	53.39	49.41	53.5
Co (ppm)	0	0	0	0	0	0	0	0	0	0	0	0	0
Ni	0	0	10	0	0	450	590	120	0	1390	180	40	0
As	0	150	0	0	0	340	170	120	160	310	0	210	140
Ag	190	120	0	120	2370	190	100	0	0	0	0	460	0
Sb	30	0	330	550	300	0	0	0	540	0	350	0	0
Cu	0	0	0	400	700	140	290	0	0	0	0	270	0
Pb	4960	2360	1420	3390	1660	3690	3770	2760	2960	2920	3540	0	630
Zn	0	0	0	760	0	0	0	0	490	40	0	0	1040
Se	0	140	0	250	300	90	0	0	0	0	260	80	40
Total wt.%	100.7	100.1	100.6	100.3	100.4	99.91	99.69	99.34	99.57	99.22	100.5	99.95	99.89
Fe %at	33.15	32.62	33.51	32.86	33.15	33.65	33.81	33.08	33.79	33.56	33.39	36.93	33.11
S %at	66.74	67.32	66.45	66.96	66.66	66.21	66.04	66.85	66.10	66.27	66.51	63.02	66.80
Pb % at	0.10	0.05	0.03	0.07	0.03	0.07	0.07	0.05	0.06	0.06	0.07	0.00	0.01
Structural formulae													
Fe	0.99	0.98	1.01	0.99	0.99	1.01	1.01	0.99	1.01	1.01	1.00	1.11	0.99
S	2.00	2.02	1.99	2.01	2.00	1.99	1.98	2.01	1.98	1.99	2.00	1.89	2.00

Table 2. Electron microprobe analyses of chlorite.

	Chlorite from semi-massif ore (sample Kn5)									Chlorite from mineralized vein (sample Kim7)											
SiO_2 %	24.27	24.22	24.18	23.59	24.15	23.48	23.67	24.85	23.57	26.63	26.41	26.26	26.28	25.31	25.67	26.09	25.44	26.08	26.49	25.39	25.99
TiO_2	0.066	0.041	0.054	0.231	0.128	0.04	0.281	0.156	0.044	0.01	0.00	0.00	0.01	0.01	0.03	0.00	0.00	0.02	0.00	0.00	0.00
Al_2O_3	21.47	20.89	21.73	20.39	21.43	20.04	20.19	20.89	21.8	22.37	22.11	21.87	21.43	21.57	20.01	21.95	21.15	21.77	21.69	21.10	21.88
FeO	37.18	34.8	36.52	36.41	36.21	35.57	36.41	35.85	36.44	32.20	33.86	34.35	33.95	33.99	32.45	34.11	34.40	34.12	33.39	33.33	33.55
MnO	0.24	0.22	0.24	0.23	0.24	0.22	0.27	0.27	0.24	0.30	0.26	0.26	0.26	0.27	0.23	0.30	0.28	0.25	0.27	0.27	0.29
MgO	7.53	7.36	7.41	7.24	7.49	7.46	7.55	7.42	7.42	8.28	7.85	7.56	7.91	8.50	10.66	7.36	7.75	7.69	8.11	7.23	7.59
CaO	0.04	0.14	0.06	0.04	0.07	0.16	0.03	0.04	0.02	0.04	0.04	0.03	0.06	0.01	0.01	0.02	0.05	0.04	0.03	0.07	0.06
Na_2O	0.04	0.24	0.06	0.03	0.02	0.08	0.06	0.04	0.00	0.00	0.02	0.04	0.03	0.01	0.00	0.00	0.04	0.00	0.00	0.03	0.02
K_2O	0.04	0.10	0.09	0.07	0.06	0.12	0.06	0.04	0.03	0.01	0.02	0.01	0.02	0.02	0.01	0.01	0.03	0.00	0.01	0.01	0.02
Cr_2O_3	0.03	0.01	0.00	0.00	0.03	0.02	0.00	0.02	0.03	0.03	0.00	0.01	0.00	0.01	0.00	0.02	0.00	0.00	0.02	0.00	0.00
Sum	90.90	88.03	90.35	88.22	89.83	87.19	88.53	89.57	89.60	89.87	90.56	90.39	89.94	89.71	89.07	89.85	89.14	89.98	90.01	87.44	89.40
	Structural formulae on the basis of 28 O																				
Si	5.25	5.36	5.25	5.27	5.27	5.29	5.27	5.41	5.17	5.59	5.56	5.56	5.59	5.43	5.52	5.55	5.50	5.54	5.60	5.56	5.55
$Al^{(IV)}$	2.75	2.64	2.75	2.73	2.73	2.71	2.73	2.59	2.83	2.41	2.44	2.44	2.41	2.57	2.48	2.45	2.50	2.46	2.40	2.44	2.45
$Al^{(VI)}$	2.74	2.82	2.81	2.65	2.78	2.63	2.58	2.79	2.81	3.16	3.08	3.05	2.99	2.90	2.60	3.09	2.91	3.03	3.04	3.04	3.08
Ti	0.01	0.01	0.01	0.04	0.02	0.01	0.05	0.03	0.01	0.00	0.00	0.00	0.00	0.00	0.00	0.00	0.00	0.00	0.00	0.00	0.00
Cr	0.00	0.00	0.00	0.00	0.00	0.00	0.00	0.00	0.01	0.00	0.00	0.00	0.00	0.00	0.00	0.00	0.00	0.00	0.00	0.00	0.00
Fe^{3+}	0.00	0.05	0.02	0.00	0.04	0.00	0.00	0.13	0.00	0.42	0.34	0.33	0.31	0.18	0.07	0.35	0.22	0.32	0.35	0.32	0.34
Fe^{2+}	6.73	6.39	6.61	6.82	6.56	6.75	6.82	6.40	6.69	5.23	5.61	5.75	5.73	5.92	5.76	5.72	6.00	5.75	5.55	5.78	5.65
Mn	0.04	0.04	0.04	0.04	0.05	0.04	0.05	0.05	0.04	0.05	0.05	0.05	0.05	0.05	0.04	0.05	0.05	0.05	0.05	0.05	0.05
Mg	2.43	2.43	2.40	2.41	2.44	2.51	2.50	2.41	2.43	2.59	2.46	2.38	2.51	2.72	3.42	2.33	2.50	2.44	2.56	2.36	2.41
Ca	0.01	0.03	0.01	0.01	0.02	0.04	0.01	0.01	0.01	0.01	0.01	0.01	0.01	0.00	0.00	0.01	0.01	0.01	0.01	0.02	0.01
Na	0.03	0.21	0.05	0.03	0.02	0.07	0.05	0.03	0.00	0.00	0.01	0.03	0.03	0.01	0.00	0.00	0.04	0.00	0.00	0.03	0.02
K	0.02	0.05	0.05	0.04	0.03	0.07	0.04	0.02	0.02	0.01	0.01	0.01	0.01	0.01	0.00	0.00	0.01	0.00	0.00	0.01	0.01
Fe/Fe+Mg	0.73	0.73	0.73	0.74	0.73	0.73	0.73	0.73	0.73	0.69	0.71	0.72	0.71	0.69	0.63	0.72	0.71	0.71	0.70	0.72	0.71
T (°C)	364	352	364	362	362	359	362	347	372	325	329	330	326	342	328	331	336	331	324	330	331

4.4. Mineralizing events

Field and textural relationships show that two successive mineralizing fluids contributed to the formation of the Kettara deposit (Figure 6). (i) a first fluid led to the formation of a pyrrhotite-chalcopyrite-sphalerite-magnetite paragenesis and a quartz-chlorite gangue. This mineralogical association represents the main mineralization event in the Kettara massive sulphide deposit. It is affected by ductile deformation, marked by mylonitisation of pyrrhotite, orientation of pyrrhotite and chalcopyrite along the schistosity and shearing planes, presence of pyrrhotite with 120° triple junctions and development of kink band structures in the massive to semi massive ore, (ii) a second fluid led to the formation of pyrite and carbonates gangues. This association is affected by brittle cataclasis, and crosscut pyrrhotite mineralization.

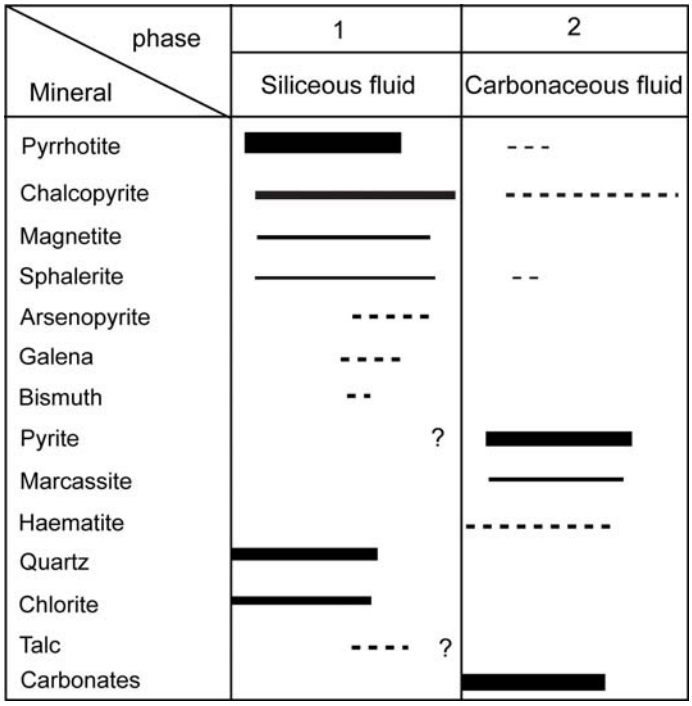

Figure 6. Paragenetic successions of the main mineralizing fluids in the Kettara massive sulphide deposit. 1 and 2 are respectively the first (pyrrhotite-rich ore) and the second (pyritic ore) main phases of mineralization

5. Fluid inclusions

Fluid inclusions were studied in the quartz of a quartz mineralized vein cut by carbonates ($V_{m\text{-}qc}$) and a quartz-chlorite mineralized vein ($V_{m\text{-}qcl}$) (Figure 3b); both are part of the first mineralized event where pyrrhotite is the dominant sulphide mineral. Carbonates minerals of $V_{m\text{-}qc}$ were not suitable for fluid inclusion studies because they are less transparent and poor in fluid inclusions. Based on petrographic observations, microthermometric analysis and Raman microspectrometry, different fluid inclusion types have been distinguished and are, summarized in table 3.

According to petrographic observation, fluid inclusions in the two mineralized veins consist mainly of two phase and one phase fluid inclusions at room temperature and scarce inclusions containing a solid phase. After microthermometric and Raman microspectrometry analyses, six fluid inclusions types have been identified, not all present in the same sample. Type 1 consists of H_2O-CO_2-N_2-CH_4 fluid inclusions; type 2 inclusions are composed by CH_4-N_2-CO_2; type 3 by H_2O-salt, type 4 by H_2O-CH_4; type 5 by N_2-CH_4 and type 6 by CH_4 (Figure 7). The type 3 inclusions exist in both $V_{m\text{-}qc}$ and $V_{m\text{-}qcl}$ veins. The quartz mineralized vein crosscut by carbonates ($V_{m\text{-}qc}$) contains also types 1 and 2 whereas quartz-chlorite mineralized vein ($V_{m\text{-}qcl}$) contains the types 4, 5 and 6.

Table 3. Summary of microthermometric and Raman microspectrometric data of fluid inclusions in mineralized veins of the Kettara massive sulphide deposit. The fluid origins are indicate by (I) for primary and (II) for secondary origins.

FI Type	Range	$T_{h(gas)(l)}$ °C	$T_{h(gas)(v)}$ °C	$T_{m(CO2)}$ °C	$T_{m(ice)}$ °C	$T_{m(cl)}$ °C	$T_{h(CO2)(l)}$ °C	$T_{h(CO2)(v)}$ °C	$T_{h(l)}$ °C	$T_{h(c)}$ °C	Td °C	Salinity wt% Nacl	R_{flv} %	Taille µm	CO_2 %	N_2 %	CH_4 %	Autres
Quartz±carbonates mineralized vein (Vm-qc)																		
Type 1 (I)	*Min*				-9.1	2.9			178				5	5	8.7	0.0	8.4	
H_2O-CO_2-N_2-CH_4	*Max*				0.0	10.1			230				10	50	84.1	79.0	51.7	
	Mean				-3.6	6.2			210				5	17	44.0	34.4	21.7	
	N				18	6			15				18	18	8	8	8	
Type 2 (I)	*Min*	-99.4	-95.9											5	11.5	21.0	36.1	
CH_4-N_2-CO_2	*Max*	-70.4	-78.3											20	27.0	38.1	67.5	
	Mean	-91.4	-88.9											11	20.0	31.9	48.0	
	N	4	5											9	7	7	7	
Type 3 (I)	*Min*				-7.9				176			3.4	5	5				
H_2O	*Max*				-2.0				258			11.6	20	30				
	Mean				-4.7				223			7.4	7	11				
	N				37				32			24	50	50				
Quartz-chlorite mineralized vein (Vm-qcl)																		
Type 3 (I)	*Min*				-17.4				174			1.1	5	5				
H_2O	*Max*				-0.6				260			20.5	10	20				
	Mean				-6.3				218			9.1	7	9				
	N				43				11			43	42	41				
Type 4 (I)	*Min*				-19.2	5.8			212				5	5			100	graphite
H_2O-CH_4	*Max*				-0.3	11			376				20	20			100	
	Mean				-6.0	8.6			291				10	10			100	
	N				14	4			15				17	17			5	1
Type 5 (I)	*Min*	-121.7	-124.1											5		49.8	39.6	
N_2-CH_4	*Max*	-121.7	-105.2											18		60.4	50.2	
	Mean	-121.7	-118.5											12		55.5	44.5	
	N	1	10											9		6	6	
Type 6 (II)	*Min*	-97.4	-85.5											5			100	graphite
CH_4	*Max*	-93.4	-82											20			100	
	Mean	-96	-85											11			100	
	N	4	9											13			14	1

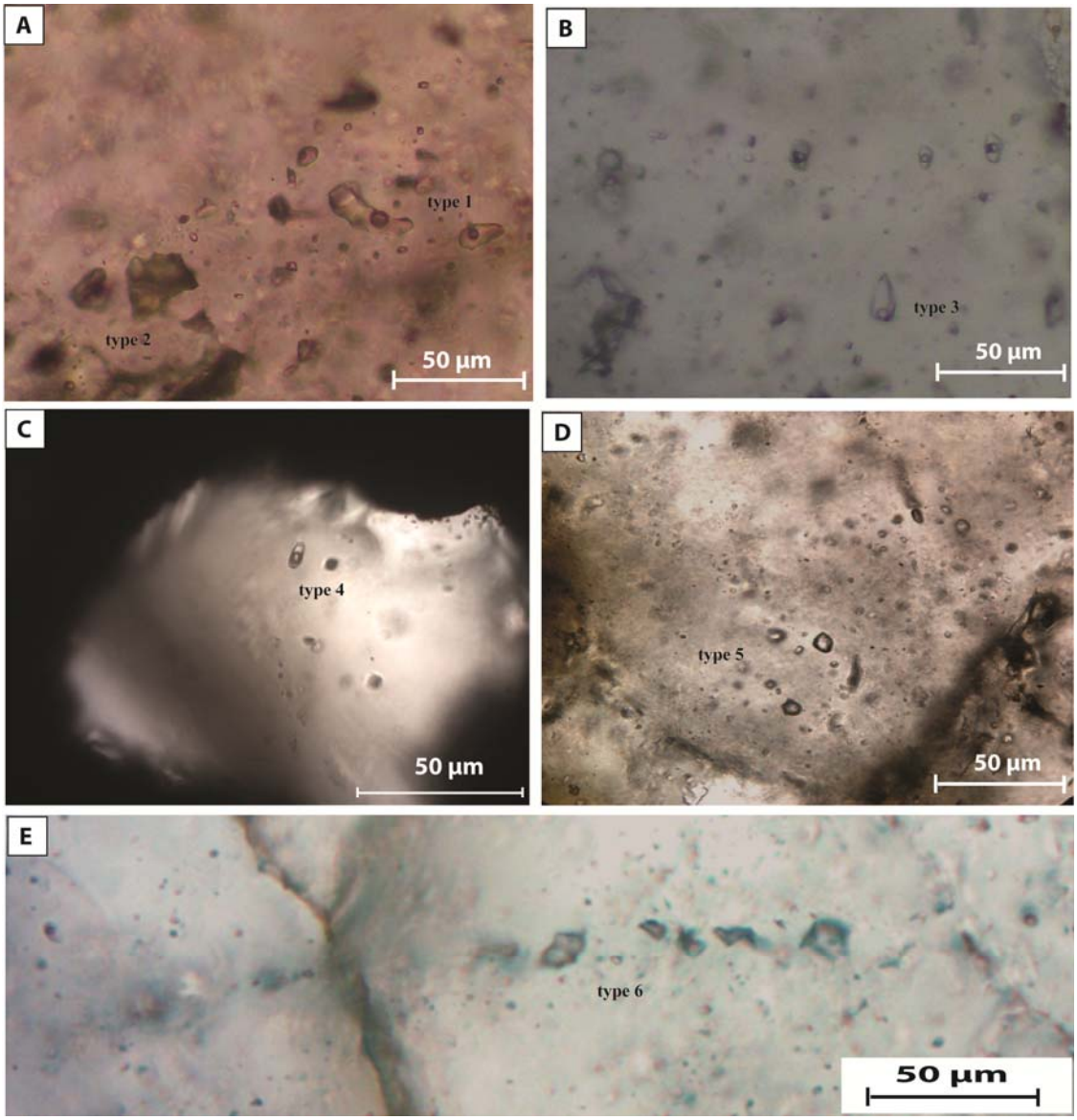

Figure 7. Photomicrographs of fluid inclusions in mineralized veins of massive sulphide in transmitted light. A) quartz mineralized vein cut by carbonates: assemblage of two phase H_2O-N_2-CO_2-CH_4 inclusions (type 1) and one phase CH_4-N_2-CO_2 inclusions (type 2). (B-E) quartz-chlorite mineralized vein, B) Two phase aqueous fluid inclusions showing a thin tip in crystal growth direction of quartz (type 3), C) two phases H_2O-CH_4-(Salt) fluid inclusions in quartz wrapped by sulphides (type 4), D) one phase N_2-CH_4 fluid inclusions (type 5), E) Secondary plan of one phase CH_4 fluid inclusions (type 6)

Type 1 inclusions are two phases at room temperature with a vapor-filling ratio (R_{Flv}) between 5 and 10%. Their size varies from 5 to 50 µm (mean of 20 µm). The inclusions have a rounded or rectangular elongated shape. In these inclusions three phase transitions have been noticed during freezing and heating runs: ice melting temperature $T_{m(ice)}$, clathrate melting temperature $T_{m(cl)}$ and bulk homogenization temperature (T_h). $T_{m(ice)}$ ranges from -9.1 to 0.0 °C with a mean value of -3.6 °C (Figure 8a), T_h are between 178 and 230 °C with an average of 210 °C (Figure 8b), and $T_{m(cl)}$ ranges from 2.9 to 10.1 °C with a mean value of 6.2 °C. The vapor phase of these inclusions is composed by variable proportions of carbon dioxide, nitrogen and methane. CO_2 and CH_4 are present in all inclusions whereas nitrogen is often missing or its content is lower than the detection limit. According to the semi-quantitative composition (*X in mole percent*) of gases calculated from Raman spectrum areas, X_{CO2} varies from 8.7 to 84.1 mol%, X_{CH4} varies from 8.4 to 51.5 mol% and when nitrogen is detected X_{N2} range from 17.9 to 79.0 mol%. Their average composition is 44.0 mol% CO_2, 21.7 mol% CH_4 and 34.4 mol% N_2.

Type 2 inclusions are one phase at room temperature and are commonly observed in the same fluid inclusion assemblages (FIA, Goldstein & Reynolds 1994) than type 1. They are less abundant and have a dark appearance with often an exceptional large size of 60 µm. No visible aqueous phase was detected during microthermometric experiments. Only T_h has been measured in these inclusions. It occurs either into liquid or vapor phase, with values of $T_{h(L)}$ ranging from -99.4 to -70.4 °C (mean = -91.4 °C) and $T_{h(V)}$ from -95.9 to -78.3 °C (mean = -88.9 °C) (Figure 8c). Raman analysis shows that they are composed of CO_2 (from 11.5 to 27.0 mol%), N_2 (from 21.0 to 38.1 mol%) and CH_4 (from 36.1 to 67.5 mol %). The mean values of these gas show the predominance of methane (X_{CH4} = 48.0 mol%) followed by nitrogen (X_{N2} = 31.9 mol%) and then by carbon dioxide (X_{CO2} = 20.0 mol%).

Type 3 inclusions exist in both the quartz mineralized vein cut by carbonates ($V_{m\text{-}qc}$) and in the quartz-chlorite mineralized vein ($V_{m\text{-}qcl}$). They have a bright aspect and contain two phases at room temperature. In $V_{m\text{-}qc}$ their size is generally about 5 to 30 µm with relatively large R_{Flv} (5 to 20%). In $V_{m\text{-}qcl}$ they have an irregular shape with sometimes a thin tip oriented in the crystal growth direction which could indicate a primary origin of these inclusions; their R_{Flv} range from 5 to 10%. The $T_{m(ice)}$ are between -7.9 and -2.0 °C in $V_{m\text{-}qc}$ and between -17.4 and -0.6 °C in $V_{m\text{-}qcl}$, with mean values of -4.7 and -6.3 °C respectively (Figure 8e). Their T_h range from 176 to 258 °C (mean = 224 °C) for $V_{m\text{-}qc}$ and from 174 to 260 °C (mean = 218 °C) for $V_{m\text{-}qcl}$ (Figure 8f). So, in $V_{m\text{-}qc}$ salinities are between 3.4 and 11.6 wt% NaCl eq. and in $V_{m\text{-}qcl}$ they range from 1.1 to 20.5 wt% NaCl eq. According to the frequency plot of $T_{m(ice)}$ (Figure 8e), the maximal frequency of $T_{m(ice)}$ corresponds to the mean value in $V_{m\text{-}qc}$ (-4.7 °C), whereas in $V_{m\text{-}qcl}$ the value of maximal frequency is a bit lower than the mean value and is around -5.0 °C. The salinities from these values are 6.9 and 7.9 wt % NaCl eq. respectively.

Type 4 inclusions are two phase fluid inclusions showing a regular shape. They appear dark and are particularly abundant in quartz wrapped by sulphides. Their average size is about 10 µm with an R_{Flv} around 5 and 20 %. One inclusion of this group contains exceptionally a solid phase which is considered as accidental solid according to the lack of other solid phases in its surrounding inclusions. $T_{m(ice)}$ range from -19.2 to -0.3 °C with a mean value of -6.0 °C (Figure 8a). T_h range from 212 up to 376 °C with a mean value around 290°C (Figure 8b), and $T_{m(cl)}$ has a mean value of 8.6 °C. The Raman analysis indicates that the vapor phase is composed exclusively of methane and the accidental solid is graphite.

Type 5 inclusions are represented by dark monophase fluid inclusions and form sometimes FIA with type 4 inclusions. They are more abundant in some quartz crystals and have a sub-regular shape. During cooling runs these inclusions showed only a $T_{h(V)}$ ranging from -124.1 to -105.2 °C with a mean value of -120 °C, and one $T_{h(L)}$ observed at -121.1 °C (Figure 8c). The Raman analysis indicates the presence of nitrogen and methane with X_{N2} varying between 49.8 and 60.4 mol% and X_{CH4} between 39.6 and 50.2 mol%. The T_h range (-124.1 to -105.2°C) indicates low bulk densities (0.07 to 0.12 g/cm^3) (Thiéry *et al.* 1994).

Type 6 inclusions consist of monophase secondary fluid inclusions located along transgranular trails with inclusion sizes reaching 40 µm. As in type 4 inclusions, one inclusion of this group contains an accidental solid. Their microthermometric data are: $T_{h(CH4)(L)}$ between -97.4 and -93.4 °C and $T_{h(CH4)(V)}$ between -85.5 and -82.0 °C (Figure 8d). This higher limit (-82.0 °C) is almost equal to the critical temperature of methane ($T_{critical}$ = -82.1 °C, Ruano 2008). The Raman analysis indicates that these inclusions are filled only by CH_4 and that the accidental solid is graphite.

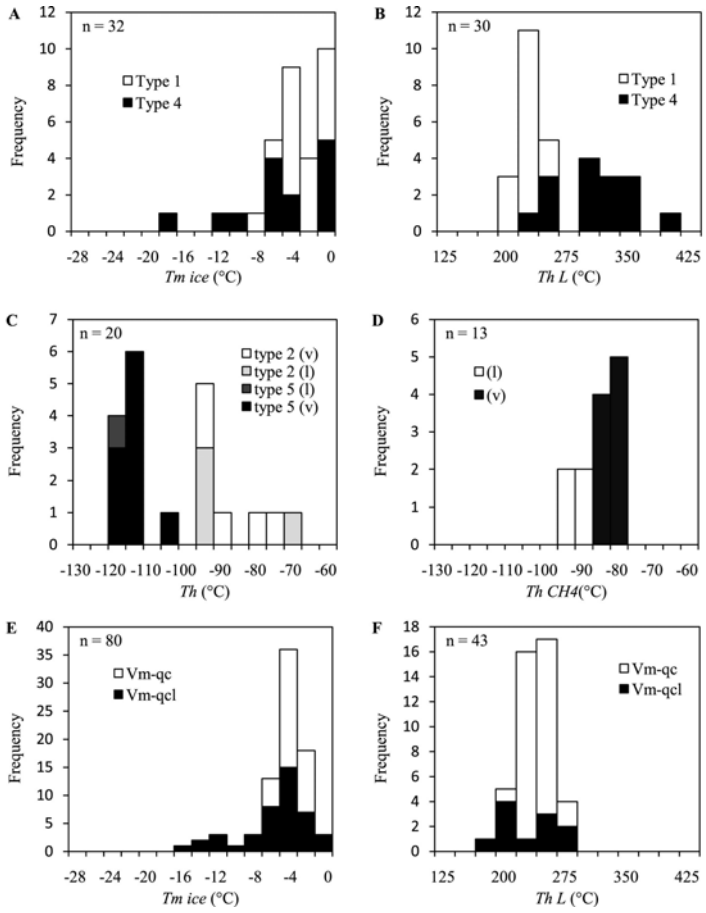

Figure 8. Histogram frequency of microthermometric data of fluid inclusions in mineralized veins of the Kettara massive sulphide. (a-b)$T_{m(ice)}$ (a) and T_h (b) of aqueous gas-bearing fluid inclusions (type 1 and 4). (c-d) T_h of gas-rich fluid inclusions (type 2, 5 and 6). (e-f) $T_{m(ice)}$ (e) and T_h (f) of aqueous fluid inclusions (type 3). Homogenization occurs into liquid phase (l) or vapor phase (v). $V_{m\text{-}qc}$: quartz mineralized vein cut by carbonates, $V_{m\text{-}qcl}$: quartz-chlorite mineralized vein

6. Discussion

6.1. General features and sources of fluid inclusions

The main systems encountered in the studied mineralized veins belong to the H_2O-(CO_2,-N_2-CH_4)±Salt, CO_2-N_2-CH_4, H_2O-(Salt), H_2O-CH_4±Salt, N_2-CH_4 and CH_4 systems. These systems can be linked to 3 main fluid types that are: 1/ a H_2O-salt fluid with variable salinities, 2/ a volatile-rich (CH_4-N_2-CO_2) fluid with variable proportions of each component ranging from pure component (pure CH_4), binary mixtures (CH_4-N_2) to ternary mixtures (CO_2-CH_4-N_2), 3/ a mixed H_2O-salt-volatiles fluid. The volatile content of the two types of mineralized veins is always dominated by CH_4 or a mixture of CH_4 and N_2, whereas CO_2 is in minor proportions or absent (Figure 9). CH_4 and CH_4-N_2 indicate reducing conditions which seem to characterize the ore-associated veins. Note that H_2S was never found whatever the context. These fluids can be linked to three distinct sources: (i) metamorphic fluids (H_2O-CO_2-CH_4-N_2), (ii) magmatic fluids (H_2O - Salt (Na, K, Li)) and (iii) fluids of basins (H_2O-gaz-(hydrocarbon)-Salt) (Cathelineau *et al.* 2011). According to Thiéry *et al.* (1994), the ternary CO_2-CH_4-N_2 system is common in fluid inclusions representative of diagenetic, hydrothermal and metamorphic fluids.

The variability of compositions, homogenization temperatures and salinities can be attributed to three main phenomena that are cooling, boiling or mixing of fluids, in addition to post-trapping processes. The graphical representation of T_h versus $T_{m(ice)}$ of fluid inclusions containing an aqueous phase allows us to identify the major trends of these mechanisms (Figure 10).

In the quartz mineralized vein crosscut by carbonates ($V_{m\text{-}qc}$), the co-existence of water+volatile (H_2O-CO_2-N_2-CH_4, type 1) and volatile-rich (CH_4-N_2-CO_2, type 2) inclusions in the same FIA is probably an indication of

boiling or mixing. This hypothesis is corroborated by the slight evolution of $T_{m(ice)}$ relative to T_h, (Figure 10a). In addition, the composition of the vapor phase (CH_4-N_2-CO_2) of type 1 inclusions is similar to type 2. Final homogenization temperatures of type 1 and type 3 inclusions are almost identical (210 and 220 °C respectively), which testifies in favour of a boiling process by which the separation of volatile phases from the liquid phase occurred causing the salt concentration in the residual liquid. Fluid inclusions resulting by this process give a similar T_h range. So, the T_h of both types (210-220°C) can be considered as the minimal trapping temperature of the inclusions.

In the quartz-chlorite mineralized vein ($V_{m\text{-}qcl}$), there is a linear distribution of type 3 and type 4 fluid inclusions along the T_h axis indicating a more significant variation of T_h than salinities. This distribution mode is characteristic of cooling for both fluid inclusion types (Figure 10b). On the other side, we also observe that relatively high T_h are recorded by type 4 fluid inclusions (up to 370 ° C) compared to type 3 (< 270 °C). This highest T_h suggests the trapping of two immiscible phases in type 4 inclusions (H_2O-CH_4) and indicates a mixing process probably between those of type 3 (H_2O) and type 5 (N_2-CH_4). After Holloway (1984), the immiscibility between CH_4 and H_2O could result in the common occurrence of methane as natural gas in low-grade metamorphic terranes. Otherwise, the missing of N_2 in type 4 inclusions is still unexplained. Post-trapping alteration of inclusions cannot be ruled out, particularly the water leakage outside inclusions. However data obtained on gas-bearing inclusions give consistent densities inside a given FIA, which argues against water leakage.

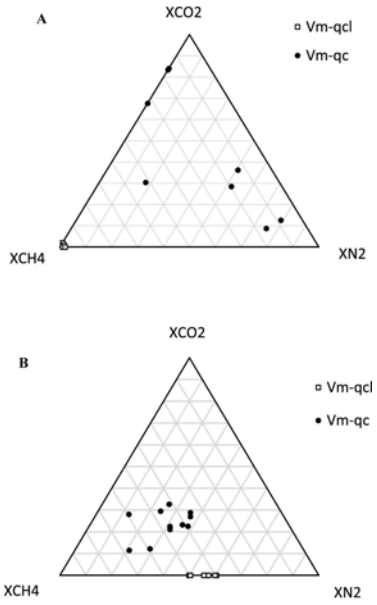

Figure 9. Ternary diagram showing the repartition of gas phases in fluid inclusions of mineralized veins of Kettara massive sulphide. A) Aqueous gas-bearing inclusions (H_2O-gas-(Salt)), type 1 and type 4 of all veins) showing a sparse repartition of gases. B) Gas-rich fluid inclusions (type 2 of all veins and type 5 and type 6 in $V_{m\text{-}qcl}$) showing the prevalence of CH_4 and N_2than CO_2. $V_{m\text{-}qc}$: quartz mineralized vein cut by carbonates, $V_{m\text{-}qcl}$: quartz-chlorite mineralized vein

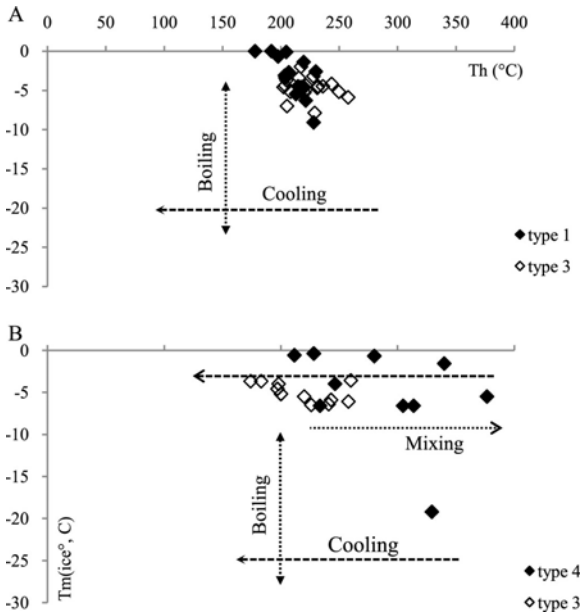

Figure 10. Plot of representative microthermometric data of type 1 and type 3 fluid inclusions in $T_h$vs$T_{m(ice)}$ binary diagram. A) From quartz mineralized vein cut by carbonates, B) From quartz-chlorite mineralized vein (see description in the text)

6.2. P-T conditions of ore formation

The quartz-chlorite mineralized vein ($V_{m\text{-}qcl}$) hosts the same paragenetic association as the massive pyrrhotitic ore and presents clear geometric relationships with the host rocks indicating syntectonic formation of the vein as described above (Figure 3b). Fluid inclusions data from this vein is then used to constrain the general evolution of the main mineralization (pyrrhotite-rich mineralization) in the Kettara massive sulphide deposit. Isochores were calculated using published equations of state suitable for the different systems that have been identified using technical characterization applied on fluid inclusions. The choice of the equation of state according to the fluid compositions and P-T conditions of validity was made using the software GEOPROFI (Pernot & Dubois 2007).

If we assume a mixing process between an aqueous fluid and a volatile-bearing fluid in $V_{m\text{-}qcl}$, the resulting fluid would be probably in an immiscible state (saturation of water relative to $CH_4 \pm N_2$) that can influence the final homogenisation temperature of aqueous gas-bearing fluid inclusions. Otherwise, chlorite geothermometry indicates temperatures between 325 and 342 °C (Kranidiotis & Mac Lean 1987) for chlorites of the mineralized vein. A temperature of 330 °C can then be used to constrain the *P-T* conditions of emplacement of the pyrrhotite mineralization. Intersection of this temperature with the batch of isochoric curves of the aqueous gas-free inclusions (type 3), calculated using the model of Zhang & Frantz (1987), gives pressure between 1.4-2.8 kbar, with a mean of c. 2 kbar (Figure 11). Intersection with the isochores of the primary gas-bearing fluid inclusions (type 5), calculated using the GEOPROFI software (Pernot & Dubois 2007) with the equation of state of Bakker (1999) gives unrealistic pressures, because of the surprisingly low density of the inclusions. Finally the system was lately invaded by a CH_4-bearing fluid, as recorded in clearly secondary fluid inclusions (type 6). Densities (0.22 to 0.23 g/cm^3) were calculated using a polynomial fit of the data from Angus *et al.* (1976). The corresponding pressure (≈250 à 500 bar) is low as shown by the isochores calculated using the equation of state of Jacobs & Kerrick (1981) (Figure 11).

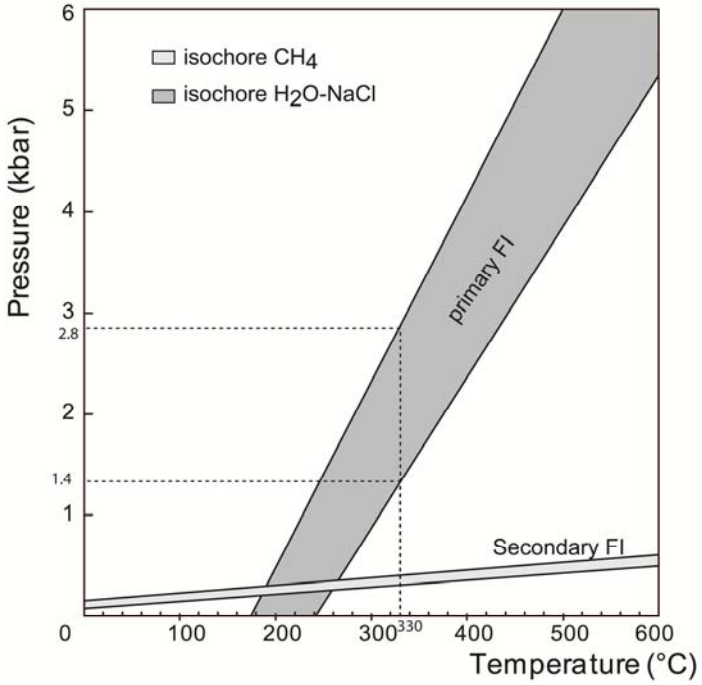

Figure 11. Representative isochores of the fluid inclusions in quartz-chlorite veins. Isochores of two phase aqueous gas-free fluid inclusions (type 3) are calculated after the model of Zhang and Frantz (1987) and isochors of one phase methane-rich inclusions (type 4) are calculated after the equation of state of Jacobs and Kerrick (1981) using the software GEOPROFI (Pernot and Dubois 2007)

6.3. Origin and timing of the mineralizing fluids

Mineralization in the Kettara deposit is essentially composed of two mineralization occurrences (Figure 6). The first is dominated by pyrrhotite associated with chalcopyrite-sphalerite-magnetite and a quartz-chlorite gangue, and is affected by ductile deformation. The second is dominated by pyrite associated with carbonates and is affected only by brittle to semi-brittle deformation.

The first mineralizing fluid which generated the main pyrrhotite-rich mineralization of the Kettara massive sulphide deposit was most likely emplaced by replacement of the host rocks. The presence of schist fragments and dolerite lenses (Huvelin 1970) inside the massive sulphide lens is consistent with a replacement process. The selective replacement of pelite layers in the wall rocks by sulphides (figure 3b) is also consistent with such a process. Because pyrrhotite is affected by ductile deformation, its deposition could be either pre- or syn-deformational. Post-depositional textures like annealing (120° triple junctions) is generally taken as an argument for pre-metamorphic deposition of sulphides, however they can occur with also fracture-filling textures (remobilized chalcopyrite) during late deformation stages affecting massive sulphides (e.g. Kuşcu & Erler 2002). According to this, syn-deformational mineralization and/or mineralization formed during prograde metamorphism (Pohl 1992; Marshall & Spry 1998) could also show theses textures.

The second mineralizing fluid, which generated the pyrite mineralization of the Kettara deposit, was emplaced by replacement of the pyrrhotite mineralization and its wall rocks. Because pyrite mineralization is only affected by brittle cataclasis, it was strong probably emplaced during the waning stages of deformation.

Fluid inclusion compositions (H_2O, CO_2, N_2, CH_4) of the main mineralizing fluid, i.e. the first fluid, and *P-T* conditions of their entrapment (c. 2 kbar) are consistent with a metamorphic context. T_h (174 to 370 °C) and salinities (7.5 wt.% NaCl) at Kettara deposit are different from SEDEX-type deposits where the fluid temperature (90 - 200 °C; Jébrak & Marcoux 2008) can reach 260 °C (*e.g.* Kamona 2011) and salinities range from 8 to more than 25 wt.% NaCl eq. (*e.g.* Leach *et al.* 2005). The calculated pressure for the main pyrrhotite mineralization of the Kettara deposit (c. 2 kbar) is higher than pressures of formation of VMS-type deposits (<1 kb; Jébrak & Marcoux 2008). The volatile content of the gas-bearing monophase inclusions in the quartz-chlorite mineralized vein (100 mol% CH_4 or 56 mol% N_2 - 44 mol% CH_4) and the quartz mineralized vein crosscut by carbonates (48 mol% CH_4 - 32 mol% N_2 – 20 mol% CO_2) are not consistent with volcanic-associated massive

sulphide deposits where inclusions are dominantly aqueous (Wilkinson 2001). The presence of such volatiles in the mineralizing fluid indicates reducing conditions. N_2 generally originates from 3 different sources: 1) atmosphere, 2) phyllosilicates after transformation of NH_4^+ into N_2 (Bastoul *et al.* 1992), and 3) mantle. In the present case the source is probably the country rocks from which N_2 could be released during progressive metamorphism. The aqueous gas-bearing fluid inclusions (H_2O-CO_2-CH_4-N_2) of the quartz mineralized vein crosscut by carbonates are characteristic of metamorphic fluids (Roedder 1984). The gas free aqueous fluid inclusions yield low salinities (mean = 7.5 wt.% NaCl eq.) typical for low grade metamorphic rocks and consistent with early dehydration of the metasedimentary sequence during deformation (Kerrich 1986; Goldfarb *et al.* 1988; Seccombe 1990; Wilkinson 2001).

Otherwise, chlorite geothermometry (325-370 °C) and fluid inclusion data allow us to propose the formation of the Kettara main mineralization at c. 200-400 °C and c. 2 kb. These parameters indicate that the emplacement of the deposit might be occurred either in transition between diagenetic and metamorphic conditions or in metamorphic conditions. Indeed, the onset of metamorphosis, which begins between 200 and 350 °C, overlaps the upper temperature range for diagenesis (Holloway & Dahlgren 2002).

7. Conclusion

The Kettara deposit is a pyrrhotite-rich massive sulphide deposit hosted by metasedimentary rocks intruded by syntectonic plutonic rocks. The deposit is formed by the superposition of two mineralogical assemblages. The main paragenesis is pyrrhotite-rich and is accompanied by chalcopyrite, magnetite, sphalerite, arsenopyrite and galena, associated essentially with a quartz-chlorite gangue. The presence of magnetite in this paragenesis indicates that the main mineralizing fluid was Fe-rich. The second paragenesis is pyrite-rich. It is accompanied by marcasite and it was generated by replacement of the pyrrhotite-rich mineralization and its wall rocks by carbonates. The first mineralized paragenesis is affected by ductile deformation whereas the second is affected only by brittle to semi-brittle deformation.

Fluid inclusions data indicate that the mineralizing fluid associated to pyrrhotite formation is characterized by H_2O, CO_2, CH_4 and N_2 volatiles, salinities of 7.5 wt.% NaCl eq. and T_h ranging from 170 to 370 °C. Chlorite geothermometry of chlorites associated to the main mineralization indicates they were formed at temperatures between of 325 and 370 °C. According to the structural and textural observations, fluid inclusions studies and chlorite geochemistry, we concluded that the main mineralization of the Kettara deposit would have been formed at 200-400 ° C and c. 2 kbar under reducing conditions. This event took place either in transition between diagenetic and metamorphic environment or in metamorphic environment by selective replacement of host rocks by the mineralizing fluid.

Acknowledgements

Ouadjou A. and Radnaoui A. from Managem group and Mouttaqi A. from ONHYM are thanked for providing geological data of the Kettara abandoned mine. Goodenough K. M. From British Geological Survey is also thanked for constructive comments on an earlier version of this manuscript. This work was partially financed by the project URAC 43.

References

Agard, J., Destombes, J. & Van Leckwijck, W. (1952). Géologie de gîtes minéraux marocains, Fer. *Notes et Mém Serv Géol Maroc* **87**, 128–128.

Angus, S., Armstrong, B. & De Reuck, K. M. (1976). International thermodynamic tables of the fluid state - 5 Methane. Chemical Data Series, 20. Chemical Data Series 20. New York: Pergamon Press.

Arnold, R. G. (1966). Mixtures of hexagonal and monoclinic pyrrhotite and the measurement of the metal content of pyrrhotite by X-RAY diffraction. *The American Mineralogist* **51**, 1221–1227.

Bakker, R. J. (1999). Adaptation of the Bowers and Helgeson (1983) equation of state to the H2O-CO2-CH4-N2-NaCl system. *Chemical Geology* **154**, 225–236.

Barton, P. B. J. (1978). Some ore textures involving sphalerite from the Furutobe mine, Akita Prefecture, Japan. *Mining Geology* **28**, 293–300.

Bastoul, A., Pironon, J., Mosbah, M., Dubois, M. & Cuney, M. (1993). In-situ analysis of nitrogen in minerals. *European Journal of Mineralogy* **5**, 233–243.

Beauchamp, J. (1984). Le carbonifère inférieur des Jebilet et de l'Atlas de Marrakech (Maroc) : migration et comblement d'un bassin marin. *Bull Soc Geol Fr* **7**, 1025–1032.

Belkabir, A., Gibson, H. L., Marcoux, E., Lentz, D. & Rziki, S. (2008). Geology and wall rock alteration at the Hercynian Draa Sfar Zn–Pb–Cu massive sulphide deposit, Morocco. *Ore Geology Reviews* **33**, 280–306.

Bernard, A. J., Maier, O. W. & Mellal, A. (1988). Aperçu sur les amas sulfurés massifs des hercynides Marocaines. *Mineralium Deposita* **23**, 104–114.

Bodnar, R. J. (1993). Revised equation and table for determining the freezing point depression of H2O-NaCl solutions. *Geochimica et Cosmochimica Acta* **57**, 683–684.

Bodnar, R. J. & Vityk, M. O. (1994). Intrepretation of Microthrermometric Data for H2O-NaCl Fluid Inclusions. In: De Vivo, B. & Frezzotti, M. L. (eds) *Fluid Inclusions in Minerals, Methodes and Apllications*. Blacksburg, VA: Virginia Tech, 117–130.

Bordonaro, M. (1983). Tectonique et petrographie du district à pyrrhotine de Kettara (Paléozoïque des Jebilets, Maroc). *Unpublished 3rd cycle thesis*, Luis Pasteur Cadi Ayyad University, Strasbourg, 132p.

Bouabdelli, M. & Piqué, A. (1996). Du bassin sur décrochement au bassin d'avant pays : Dynamique du bassin d'Azrou Khenifra (Maroc Hercynien Central). *Journal of African Earth Sciences* **23**, 213–224.

Brown, D. & Mcclay, K. R. (1993). Deformation textures in pyrite from the Vangorda Pb-Zn-Ag deposit, Yukon, Canada. *Mineralogical Magazine* **57**, 55–66.

Cathelineau, M., Boiron, M.-C. & Tuduri, J. (2011). Fluides et genèse des concentrations minérales. *Geosciences* **13**, 56–63.

Essaifi, A., Capdevila, R. & Lagarde, J.-L. (1995). Transformation des leucogabbros en chloritoschistes sous leffet de l'altération hydrothermale et de la déformation dans l'intrusion de kettara (jebilet, Marco). *C. R . Acad. Sci. Paris, Série IIa, t.* **320**, 189–196.

Essaifi, A., Lagarde, J.-L. & Capdevila, R. (2001). Deformation and displacement from shear zone patterns in the Variscan upper crust , Jebilet , Morocco. *Journal of African Earth Sciences* **32**, 335–350.

Essaifi, A., Capdevila, R., Fourcade, S., Lagarde, J.-L., Ballèvre, M. & Marignac, C. (2004). Hydrothermal alteration, fluid flow and volume change in shear zones: the layered mafic-ultramafic Kettara intrusion (Jebilet Massif, Variscan belt, Morocco). *Journal of Metamorphic Geology* **22**, 25–43.

Essaifi, A. & Hibti, M. (2008). The hydrothermal system of Central Jebilet (Variscan Belt, Morocco): A genetic association between bimodal plutonism and massive sulphide deposits? *Journal of African Earth Sciences* **50**, 188–203.

Essaifi, A. (2011). L'ancienne mine de pyrrhotine de Kettara. In Michard et al. (eds.), Nouveaux guides géologiques et miniers du Maroc, vol. 9. *Notes et Mém Ser Géol Maroc* **563**, 71–82.

Essaifi, A., Samson, S. & Goodenough, K. (2014). Geochemical and Sr–Nd isotopic constraints on the petrogenesis and geodynamic significance of the Jebilet magmatism (Variscan Belt, Morocco). *Geological Magazine* **151**, 666–691.

Fournier, M., Felenc, J. & Hmeurras, M. (1987). Un amas sulfuré à pyrrhotine en milieu sédimentaire Kettara (Jébilets) - Maroc. *Rapport BRGM*, 77p.

Frezzotti, M. L., Tecce, F. & Casagli, A. (2012). Raman spectroscopy for fluid inclusion analysis. *Journal of Geochemical Exploration*. Elsevier B.V. **112**, 1–20.

Goldfarb, R., Leach, D., Picktorn, W. & Paterson, C. (1988). Origin of lode-gold deposits of the Juneau gold belt, southeastern Alaska. *Geology* **16**, 440–443.

Hibti, M., Bouabdelli, M., Mouttaqi, A., Sagon, J.-P. (1999). L'effet du métamorphisme sur les minéralisations sulfurés de la province hercynienne (Meseta sud-occidentale, Maroc). Exemple des gisement sulfuré de Hajjar et de Kettara. *Chronique de la Recherche Minière* **536-537**, 23–37.

Hibti, M. & Marignac, C. (2001). The Hajjar deposit of guemassa (SW Meseta, Morocco) : a metamorphosed syn-sedimentary massive sulphide ore body of the Iberian type of volcano-sedimentary massive sulphide deposit. In: Piestrzyński et al (ed.) *Mineralium Deposita at the Beginning of the 21st Century*. Sweet & Zeitlinger Publishers Lisse, 281–284.

Hoepffner, C., Houari, M. & Bouabdelli, M. (2006). Tectonics of the North African Variscides (Morocco, Western Algeria), an outline. In: Frizon de Lamotte, D., Saddiqi, O. & Michard, A. (eds) *Recent Developments on the Maghreb Geodynamics*. Compte Rendu Geoscience, 25–40.

Holloway, J. R. (1984). Graphite-CH4-H2O-CO2 equilibria at low-grade metamorphic conditions. *Geology* **12**, 455–458.

Holloway, J. M. & Dahlgren, R. A. (2002). Nitrogen in rock: Occurrences and biogeochemical implications. *Global Biogeochemical Cycles* **16**(4), 1–17.

Huvelin, P. (1970). Amas sulfuré à pyrrhotine dans les schistes carbonifères du district des gabbros de la région de Kettara (Jebilet, Maroc). *C. R . Acad Sci. Paris, Série II, t.* **270**, 2717–2520.

Huvelin, P. (1977). Etude géologique et gîtologique du Massif hercynien des Jebilet (Maroc occidental). *Notes Mém Serv Géol Maroc* **232 bis**, 1–307.

Jacobs, G. & Kerrick, D. (1981). Methane: an equation of state with application to the ternary system H2O-CO2-CH4. *Geochimica et Cosmochimica Acta* **45**, 607–614.

Jébrak, M. & Marcoux, E. (2008). *Géologie des Ressources*. GÉOLOGIE QUÉBEC, 667.

Kamona, F. (2011). Carbonate-Hosted Base Metal Deposits. In: Dr. Imran Ahmad Dar (eds) Earth and Environmental Sciences. ISBN: 978-953-307-468-9. InTech, Available from: http://www.intechopen.com/books/earth- and-environmental-sciences/carbonate-hosted-base-metal-deposit

Kerrich, R. (1986). Fluid transport in lineaments. *Phil Trans Lond* **A** 317:219–251.

Kranidiotis, P. & Mac Lean, W.H. (1987). Systematics of chlorite alteration at the Phelps Dodge massive sulfide deposit, Matagami, Quebec. *Economic Geology* **82**,1898–1911.

Kuşcu, L., Erler, A. (2002). Pyrite Deformation Textures in the Deposits of the Küre Mining District (Kastamonu-Turkey). Turkish J of Earth Sci **11**, 205-215.

Lagarde, J.-L. & Choukroune, P. (1982). Cisaillement ductile et granitoïdes syntectoniques : l'exemple du massif hercynien des Jebilet (Maroc). *Bull Soc Géol Fr* **24**, 299–307.

Le Corre, C. & Bouloton, J. (1987). Un modèle de "'structure en fleur'" associant décrochement et convergence: Les Jebilet centro-occidentales (Maroc hercynien). *CR Acad Sci Paris Série II* **13**, 751–755.

Leach, D. L., Sangster, D. F., Kelley, K. D., Large, R. R., Garven, G., Allen, C. R., Gutzmer, J. & Walters, S. (2005). Sediment-Hosted Lead-Zinc Deposits: A Global Perspective. *Economic Geology* **100th Anni**, 561–607.

Lotfi, F., Belkabir, A., Brown, A. C., Marcoux, E., Brunet, S. & Maacha, L. (2008). Geology and Mineralogy of the Hercynian Koudiat Aïcha Polymetallic (Zn-Pb-Cu) Massive Sulfide Deposit , Central Jebilet , Morocco. *Exploration and Mining Geology* **17**, 145–162.

Marcoux, E., Belkabir, A., Gibson, H. L., Lentz, D. & Ruffet, G. (2008). Draa Sfar, Morocco: A Visean (331 Ma) pyrrhotite-rich, polymetallic volcanogenic massive sulphide deposit in a Hercynian sediment-dominant terrane. *Ore Geology Reviews* **33**, 307–328.

Marshall, B., Spry, P.G. (1998). Discriminating between regional metamorphic remobilization and syn-tectonic emplacement in the genesis of massive sulfide ores. In: Vokes FM, Marshall B, Spry PG (eds) Metamorphic and Metamorphogenic Ore Deposits. *Reviews in Economic Geology* **11**, 39-80.

Moreno, C., Sáez, R., González, F., Almodóvar, G., Toscano, M., Playford, G., Alansari, a., Rziki, S. & Bajddi, A. (2008). Age and depositional environment of the Draa Sfar massive sulfide deposit, Morocco. *Mineralium Deposita* **43**, 891–911.

Mrini, Z., Rafi, A., Duthou, J. L. & Vidal, P. (1992). Chronologie Rb-Sr des granitoïdes hercyniens du Maroc: conséquences. *Bulletin de la Société Géologique de France* **163**, 281–91.

Pernot, N. & Dubois, M. (2007). GEOPROFI : An evolutionary software to calculated inclusions isochores from equations of state. In: Diamon LW, Pettke T, Spandler C (eds). *ECROFI XIX*, Bern (Switzerland), pp. 138

Piqué, A. & Michard, A. (1989). Moroccan hercynides, a synopsis. The paleozoic sedimentary and tectonic evolution at the northern margin of West Africa. *Am J Sci* **298**, 286–330.

Pohl, W. (1992). Defining metamorphogenic mineral deposits-an introduction. *Mineralogy and Petrology* **45**, 145–152.

Poty, B., Leroy, J. & Jachimowicz, L. (1976). Un nouvel appareil pour la mesure de températures sous le microscope : l'installation de microthermométrie Chaixmeca. *Bull Soc Fr Minéral Cristallogr* **9**, 182–186.

Roedder, E. (1984). Fluid inclusions. Reviews in Mineralogy 12. *Mineralogical Society of America*, pp 646

Ruano, S. M. (2008). Analytical techniques applied to fluid inclusion studies: basics and applications. In: Subías, I. & Bauluz, B. (eds) *Tech. Appl. TO Mineral. GEOCHEMISTRY, SEMINARIOS*. Spain, 133–154.

Seccombe, P. (1990). Fluid inclusion and sulphur isotope evidence for syntectonic mineralization at the Elura mine, southestern Australia. *Mineralium Deposita* **25**, 304–312.

Souaré, A. (1988). Contribution à l'étude des amas sulfurés du district des Jebilet centrales et de leurs altérations supergènes, (chapeau de fer) comparaison avec les minéralisations sulfurées d'Agouim (Haut Atlas, Maroc). *Unpublished 3rd cycle thesis*, Cadi Ayyad University, Marrakech, 273p.

Thiéry, R., Vidal, J. & Dubessy, J. (1994). Phase equilibria modelling applied to fluid inclusions: Liquid-vapour equilibria and calculation of the molar volume in the CO2-CH4-N2 system. *Geochimica et Cosmochimica Acta* **58**, 1073–1082.

Vaughan, D.J. & Craig, J.R. (1978). Mineral Chemistry of the Metal Sulphides. *Cambridge University Press*, Cambridge

Wilkinson, J. . (2001). Fluid inclusions in hydrothermal ore deposits. *Lithos* **55**, 229–272.

Zhang, Y.G. & Frantz, J.D. (1987). Determination of the homogenization temperatures and densities of supercritical fluids in the system NaCl-KCl-CaCl2-H2O using synthetic fluid inclusions. *Chemical Geology* **64**: 335-350.